Viscous Shock-Layer Solutions for Hypersonic Sphere Cones

B. N. Srivastava,* M. J. Werle,† and R. T. Davis‡
University of Cincinnati, Cincinnati, Ohio

Theoretical predictions of flow properties are obtained for the nose region (2-3 nose radii) of spherically blunted cones in hypersonic flow at intermediate to high Reynolds numbers. The numerical method used to obtain solutions to the shock-layer equations is discussed, with attention focused on the development of a new technique to accommodate surface curvature discontinuities and convection effects in the normal momentum equation. Solutions are presented for cone half-angles from 30 deg down to 0 deg, where previous shock-layer methods encountered severe difficulties. Comparisons are made with inviscid flow solutions, independent shock-layer solutions, and experimental data.

Nomenclature

a^* = nose radius
c^* = viscosity law constant, $c^* = 198.6°\text{R}$
C_f = skin friction coefficient, $2\tau^*/(\rho_\infty^* u_\infty^{*2})$
C_p^* = specific heat at constant pressure
H = nondimensional total enthalpy, H^*/u_∞^{*2}
k = thermal conductivity
M_∞ = freestream Mach number
n = nondimensional normal distance
n_s = shock standoff distance normal to body
p = nondimensional pressure, $p^*/(\rho_\infty^* u_\infty^{*2})$
q = nondimensional heat transfer, $q^*/(\rho_\infty^* u_\infty^{*3})$
r = nondimensional axisymmetric radius
Re_∞ = $\rho_\infty^* u_\infty^* a^*/\mu^*(u_\infty^* 2/C_p^*)$
Re_{sh} = $\rho_{sh}^* u_{sh}^* a^*/\mu_{sh}^*$
R = defined as $y_B + n_s\cos\phi$
s = nondimensional surface distance
St = Stanton number, $q_w/(H_0 - H_w)$
T = nondimensional temperature, $C_p^* T^*/u_\infty^{*2}$
u = nondimensional tangential velocity, u^*/u_∞^*
v = nondimensional normal velocity, v^*/u_∞^*
x_B = axial distance from stagnation point
y_B = normal distance for body surface measured from axis
x_s = defined as $x_B - n_s\sin\phi$
α = shock angle, see Fig. 1
β = angle defined in Fig. 1
γ = ratio of specific heats
ϵ = $[\mu^*(u_\infty^{*2}/C_p^*)/\rho_\infty^* u_\infty^* a^*]^{1/2}$
κ = nondimensional surface curvature
μ = nondimensional viscosity, $\mu^*/\mu^*(u_\infty^{*2}/C_p^*)$
ρ = nondimensional density, ρ^*/ρ_∞^*
τ = nondimensional shear stress, $\tau^*/(\rho_\infty^* u_\infty^{*2})$
ϕ = body angle defined in Fig. 1
σ = Prandtl number, $\mu^* C_p^*/k^*$

Subscripts

0 = stagnation conditions
s = used for longitudinal derivatives
sh = conditions immediately behind the shock wave
w = conditions at the body surface

Superscripts

$*$ = dimensional quantity
$-$ = normalized with shock value
j = 0 for plane flow and 1 for axisymmetric

Introduction

CURRENT interest in re-entry aerodynamics continues to draw attention to the problem of theoretically predicting the effects of hypersonic viscous flow past blunt bodies with curvature discontinuities. The simplest example of this is the spherically blunted cone configuration, and interest is focused here on the problem of predicting the detailed viscous flow structure over its nose region (2-3 nose radii) for intermediate to high Reynolds numbers.

The flow regime of interest is one in which the viscous effects influence a significant portion of the total shock-layer region between the bow shock and body, thereby violating the classical boundary-layer approximation and requiring the use of a more comprehensive set of governing equations. Three approaches for treating such problems include those employing the full Navier-Stokes equations,[1,2] the second-order boundary-layer equations,[3] or the viscous shock-layer equations.[4,5] Recent studies[6,7] indicate that the full viscous shock-layer equations (as opposed to their thin layer form) are not only convenient to use but are also sufficient to provide an accurate estimate of the flow properties for the re-entry flow conditions considered here. To date though, this method has been applied only to analytic blunt bodies for which the surface curvature was everywhere continuous and the normal convection effects in the shock layer were not dominant. The difficulties associated with the surface curvature discontinuity, such as at the sphere/cone tangency point of a spherically blunted cone, have prevented successful application of shock-layer methods to spherically blunted cones. Also, for sphere cones at intermediate to high Reynolds numbers, a significant portion of the shock layer is dominated by convection normal to the surface, especially for slender cones at hypersonic speeds. Previous studies[5,8] have experienced difficulties for such cases, prompting improvements to the solution method as summarized here and presented in Refs. 9 and 10.

This paper presents a solution method which directly accounts for surface curvature discontinuities and normal

Presented as Paper 77-693 at the AIAA 10th Fluid and Plasmadynamics Conference, Albuquerque, N. Mex., June 27-29, 1977; submitted July 12, 1977; revision received October 17, 1977.

Index categories: Viscous Nonboundary-Layer Flows; Supersonic and Hypersonic Flow; Jets, Wakes, and Viscid-Inviscid Flow Interactions.

*Graduate Research Assistant. Currently Research Engineer, Avco Everett Research Laboratory, Everett, Mass. Member AIAA.

†Professor, Dept. Aerospace Engineering and Applied Mechanics. Member AIAA.

‡Professor and Head, Dept. Aerospace Engineering and Applied Mechanics. Member AIAA.

convection effects. The procedure developed in the present approach utilizes a time-dependent relaxation technique to iterate on the bow shock shape[9,10] in order to achieve solutions of the full viscous shock-layer equations for hypersonic flow past spherically blunted cones. It is shown through this formulation that the adverse effect of the surface curvature discontinuity at the juncture point can be eliminated by carefully including in the solution procedure the necessary jump conditions associated with the longitudinal derivatives at the junction point.

Numerical solutions are generated using this approach up to about 3 nose radii for spherically blunted cones with half-angles of 30 deg, 10 deg and also for the difficult case of 0 deg (sphere cylinder) at high Reynolds numbers. The resulting surface pressures are found to compare well with independent inviscid blunt body and method of characteristics solutions when the curvature jump effects are included in the solution scheme. Solutions obtained with the jump conditions purposely misrepresented showed large errors over a significant portion of the body fore and aft of the juncture point. Proper inclusion of the jump effects is shown to provide theoretical results in excellent agreement with experimental data even at the low freestream Reynolds number of 1515 for a 7.5-deg half-angle spherically blunted cone.

Governing Equations

The viscous shock-layer concept has been presented in detail by Davis[4] and therefore is only summarized here. The compressible Navier-Stokes equations are written in a boundary-layer-like coordinate system (see Fig. 1) and nondimensionalized by variables which are of order 1 in the region near the body surface (boundary layer) for large Reynolds numbers. The same set of equations are then written in variables which are of order 1 in the essentially inviscid region outside the boundary layer. A comparison of the two sets of equations is then made and one set of equations is identified which is valid to second order in the inverse square root of a Reynolds number in both the outer (inviscid) and inner (viscous) regions. A solution to this set of equations is thus uniformly valid to second order in the entire shock layer for large Reynolds numbers. The resulting equations (and notation) are the same as those presented by Davis[4] and are given as:

Continuity

$$[(r+n\cos\phi)^j \rho u]_s + [(1+\kappa n)(r+n\cos\phi)^j \rho v]_n = 0 \quad (1a)$$

Longitudinal Momentum

$$\rho\{u\,u_s/(1+\kappa n) + v\,u_n + \kappa uv/(1+\kappa n)\} + p_s/(1+\kappa n) = [\epsilon^2/(1+\kappa n)^2 (r+n\cos\phi)^j][(1+\kappa n)^2 \cdot (r+n\cos\phi)^j \tau]_n \quad (1b)$$

where

$$\tau = \mu[u_n - \kappa u/(1+\kappa n)] \quad (1c)$$

Normal Momentum

$$\rho\{\underline{u\,v_s/(1+\kappa n)} + \underline{v\,v_n} - \kappa u^2/(1+\kappa n)\} + p_n = 0 \quad (1d)$$

where the underscored terms are ignored in the thin shock-layer approximation.

Energy Equation

$$\rho\{uT_s/(1+\kappa n) + vT_n\} - up_s/(1+\kappa n) - vp_n = \epsilon^2\tau^2/\mu + [\epsilon^2/(1+\kappa n)(r+n\cos\phi)^j][(1+\kappa n)(r+n\cos\phi)^j q]_n \quad (1e)$$

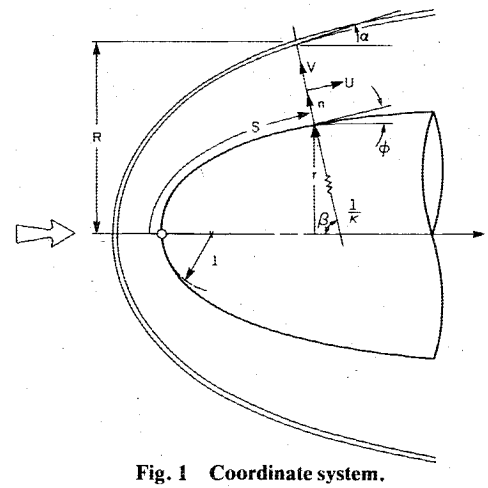

Fig. 1 Coordinate system.

where

$$q = \mu T_n/\sigma \quad (1f)$$

Equation of State

$$p = (\gamma-1)\rho T/\gamma \quad (1g)$$

Viscosity Law

$$\mu = T^{3/2}(1+c')/(T+c') \quad (1h)$$

where

$$c' = c^*/M_\infty^2 T_\infty^* (\gamma-1)$$

and c^* is taken to be 198.6°R for air.

The surface conditions employed here are the zero slip and injection conditions

$$u(s,o) = v(s,o) = 0 \text{ and } T(s,o) = T_w \quad (2)$$

while the oblique shock relations[4] are used to relate the flow variables just aft of the shock to the freestream conditions through the local shock slope. The shock angle α is related to the shock thickness n_s through the geometric relation

$$\frac{dn_s}{ds}\Big/(1+\kappa n_s) = \tan(\alpha-\phi) \quad (3)$$

where n_s is obtained from mass conservation considerations as

$$(r+n_s\cos\phi)^{1+j} = 2^j \int_0^{n_s} \rho u (r+n\cos\phi)^j dn \quad (4)$$

For computational convenience the preceding set of equations are transformed into a new set of variables by normalizing the dependent variables by their corresponding values at the shock. The resulting equations are presented by Davis.[4]

Juncture Region Analysis

Inviscid Flow Considerations

From an inviscid standpoint, it is known that a streamline curvature discontinuity produces a discontinuity in the flow gradients only along that streamline.[11] For locally supersonic flows such discontinuities would propagate along characteristic lines and its effect would eventually spread throughout the downstream flowfield through successive reflections from the bow shock and the body. This physical situation is further

complicated when the inviscid equations are expressed in a surface coordinate system. Due to the explicit appearance of the surface curvature, discontinuities occur in the coefficients of the conservation laws, and derivatives of the flow variables with respect to the surface distance undergo a discontinuous jump all along a line perpendicular to the body surface at the junction point.[10] In addition, longitudinal derivatives of the shock shape also encounter discontinuities as can be seen from the geometrical relation (Fig. 1)

$$\frac{dR}{ds} = (1+\kappa n_s)\frac{\sin\alpha}{\cos(\alpha-\phi)} \tag{5}$$

which yields a jump condition when evaluated on two sides of the juncture ($\kappa = 1$ for a sphere and $\kappa = 0$ for the cone)

$$\left(\frac{dR}{ds}\right)_{\text{sphere}} = (1+n_s)\left(\frac{dR}{ds}\right)_{\text{cone}} \tag{6}$$

Thus, solution of the viscous shock-layer equations with regions of essentially inviscid flow would require consideration of all these jump discontinuities when solved in a surface coordinate system. This is especially important to finite-difference methods which cannot accommodate discontinuities without adjustments to the difference operators.

Viscous Flow Considerations

It is important to determine what, if any, impact the viscous terms of the shock-layer equations have on the nature of the flowfield near a juncture point. It is clear that the classical boundary-layer version of the full Navier-Stokes equations cannot hold at the juncture point because both the curvature and inviscid pressure gradients encounter jump discontinuities. Any such discontinuity would be in violation of the boundary-layer scaling laws wherein longitudinal derivatives are assumed smaller than normal derivatives. It is, therefore, apparent that a new local solution needs to be developed for the junction region. Such an analysis has been performed by Messiter and Hu[12] for two-dimensional flows. Their analysis indicates that, unlike the classical boundary-layer case, in the present situation an interaction with the external flow must be taken into account, this occurring through a small pressure change acting over a suitably small distance along the boundary layer. The details of the resulting local pressure distribution cannot be specified in advance, but must be found by studying changes in the boundary layer coupled with small perturbations on the local external flow. Their formulation shows that the discontinuity in the pressure gradient predicted by the inviscid flow theory can be eliminated by using a triple-deck formulation. Continuous expressions for the pressure gradient can be obtained which are presumed to be correct asymptotic representations as the viscosity coefficient approaches zero.

These results imply two important points for the present study. First, in the sphere/cone juncture region the correct asymptotic behavior will be recovered provided the viscous set of gasdynamic equations retain the boundary-layer terms and allow for displacement interaction with the local inviscid flow. In this regard the full shock-layer equations seem to be sufficient since they contain all the viscous terms of Messiter and Hu's triple-deck model[12] plus the inertia terms that take into account the interaction effect with the inviscid flow. The second important point of interest here is that interaction effects will be significant in only a vanishingly small region of the physical flow and will be difficult to detect for high Reynolds number cases.[10]

In addition to the points presented earlier, the use of a surface coordinate system introduces new aspects of the viscous flow problem just as in the inviscid analysis presented earlier. Thus, again the question of accommodating discontinuous curvature-dependent coefficients in the governing Eqs. (1a-1e) arises. It is shown in Ref. 10 that in the viscous portions of the shock layer, the flow variables are continuous, but they still experience a discontinuity in derivatives with respect to surface distance all along a line normal to the curvature juncture point. These again will require special consideration in the solution of the full shock-layer equations.

Thin Layer Approximations

Many studies in the past have used the thin layer version of the full shock-layer equations [obtained by dropping the underscored terms in Eq. (1d)] to predict flow properties within the shock-layer region for analytic bodies.[13,14] The conclusions of the foregoing analysis are not necessarily valid for these equations due to the change in character of the governing equations from a parabolic-hyperbolic set[10,15] to a parabolic set. It was shown in Ref. 10 using integral formulation that, unlike the full set of equations, normal-shock-like discontinuity in all the flow properties may occur at the juncture point for the thin layer equations. Thus, it is concluded that further numerical studies will be needed to determine if there is a solution to the thin layer equations in surface coordinates that will carry across a point of curvature discontinuity.

Numerical Method

General Considerations

Several numerical methods have been presented for solving the thin shock-layer version of the more general shock-layer equations.[4,13,14] These approaches have two limitations. First, they are based on the assumption that the pressure gradient normal to the body surface is established entirely by centrifugal effects, and second, that the shock wave lies parallel to the body surface. In an attempt to remove these limitations, methods have been developed[4-8,16,17] for addressing the full shock-layer equations through a relaxation process wherein the thin shock-layer assumptions are removed by an iterative process. While, in general, such methods have been successful, they encounter difficulty whenever the shock-layer thickness becomes large. This difficulty usually manifests itself as a divergent behavior in the iteration scheme. In an attempt to overcome this problem, a new relaxation scheme (ADI Scheme) was developed[9] where an initial solution was relaxed in an artificial timelike manner toward the sought after steady-state solution. While application of this method to analytic body shapes was demonstrated by Srivastava et al.,[9] its extension to nonanalytic shapes with curvature discontinuities requires some improvements of the technique as presented here and in Ref. 10.

To demonstrate the present approach, the normalized version of the viscous shock-layer s-momentum equation is first rewritten using the oblique shock wave equations to obtain the form

$$\frac{\partial^2 \bar{u}}{\partial \eta^2} + \beta_1 \frac{\partial \bar{u}}{\partial \eta} + \beta_2 \frac{d^2 R}{ds^2} + \beta_3 \frac{dR}{ds} + \beta_4 + \beta_5 \frac{\partial \bar{u}}{\partial \xi} = 0 \tag{7}$$

where $\beta_1, \beta_2, \beta_3, \beta_4$, and β_5 are nonlinear coefficients as given in Ref. 10.

The present timelike relaxation scheme utilizes a two-step process somewhat similar to the alternating direction implicit method.[18] In the first step the method yields the flow variables in the shock-layer region while the second step is used to update the shock shape itself, as shown in the two-step time formulation of Eq. (7) given as

First Sweep (from $t = t^n$ to $t = t^* = t^n + \Delta t/2$)

$$\frac{\partial^2 \bar{u}^*}{\partial \eta^2} + \beta_1^* \frac{\partial \bar{u}^*}{\partial \eta} + \beta_2^* \left[\frac{\partial^2 R^n}{\partial s^2} - \frac{\partial R^*}{\partial t}\right] + \beta_3^* \frac{\partial R^n}{\partial s} + \beta_4^* + \beta_5^* \frac{\partial \bar{u}^*}{\partial \xi} = 0 \tag{8a}$$

Second Sweep (from $t=t^*$ to $t=t^{n+1}=t^*+\Delta t/2$)

$$\beta_2^*\frac{\partial^2 R^{n+1}}{\partial s^2}-\beta_2^*\frac{\partial R^{n+1}}{\partial t}+\beta_3^*\frac{\partial R^{n+1}}{\partial s}+\left[\frac{\partial^2\bar{u}}{\partial\eta^2}+\beta_1\frac{\partial\bar{u}}{\partial\eta}+\beta_5\frac{\partial\bar{u}}{\partial\xi}+\beta_4\right]^*=0 \tag{8b}$$

Note that the "steady-state" versions of these equations are precisely the "full" shock-layer equations. The boundary conditions associated with the first step [Eq. (8a)] are the familiar no-slip conditions [Eq. (2)] at the surface, and $\bar{u}=1$ at the shock location. The boundary conditions used for the second time step are the same as those used in Ref. 9 and are given as

1) at $s=0$ $\quad R=0$ (9a)

2) at $s=s_{\max}$ $\quad R^{n+1}_{\max}=R^*_{\max}$ (9b)

Two difficulties occur at a juncture point. First, the coefficients of the momentum equation as given in Eqs. (1b) and (8b) as well as the longitudinal derivatives are discontinuous across a juncture point because of a discontinuous change in the curvature κ. Further, as noted in Eq. (6), the shock derivatives are also discontinuous at the juncture. The numerical difficulty associated with Eq. (8a) can be overcome by structuring the finite-differences grid system such that the juncture point coincides with a grid point, thereby avoiding any differencing of the flow variables across the discontinuity. However, difficulty still persists with solution of Eq. (8b) since this equation requires solution of a second-order equation for a dependent variable R, whose derivatives undergo a discontinuous change at a point within the solution regime. This difficulty was overcome in the present formulation by developing finite-difference expressions of the first and second derivatives of the shock shape R that directly account for the jump conditions associated with these derivatives at the juncture point. The technique is demonstrated in the following by a simple model problem which represents the second step $(n+1)$ of the present numerical scheme as given in Eq. (8b).

Model Problem Analysis

The governing equation, boundary conditions, and associated jump conditions for a simple model problem are given as

$$\frac{d^2R}{ds^2}+\alpha_1\frac{dR}{ds}+\alpha_2 R+\alpha_3=0 \tag{10a}$$

with

$$R=0 \text{ at } s=0, \quad R=R_1 \text{ at } s=s_{\max} \tag{10b}$$

$$\left(\frac{dR}{ds}\right)_{-s_{\text{jump}}}=K_1\left(\frac{dR}{ds}\right)_{+s_{\text{jump}}} \tag{10c}$$

$$\left(\frac{d^2R}{ds^2}\right)_{-s_{\text{jump}}}=\left(\frac{d^2R}{ds^2}\right)_{+s_{\text{jump}}}+K_2\left(\frac{dR}{ds}\right)_{+s_{\text{jump}}}+K_3 \tag{10d}$$

where

$$K_2=(\alpha_1)_{+s_{\text{jump}}}-K_1(\alpha_1)_{-s_{\text{jump}}}$$

$$K_3=(\alpha_3)_{-s_{\text{jump}}}-(\alpha_3)_{+s_{\text{jump}}}$$

and K_1 is specified.

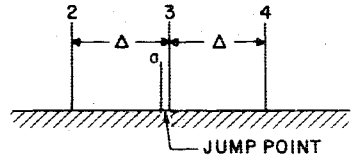

Fig. 2 Finite-difference representation.

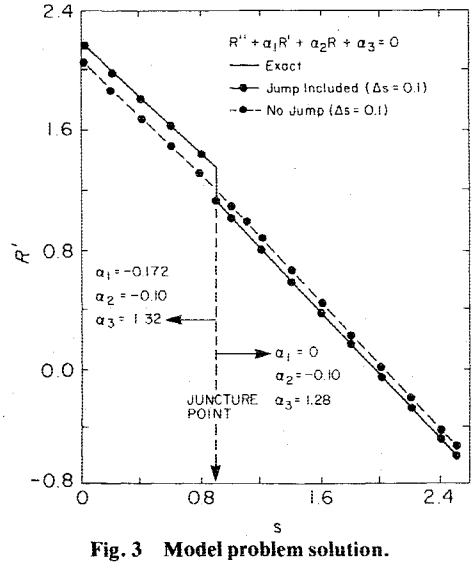

Fig. 3 Model problem solution.

For the present analysis the coefficients of Eq. (10a) will be taken to be constant but different in their respective regions before and after s_{jump} so that exact solutions can be obtained for comparative purposes. Also note that the second derivative jump condition is obtained by evaluating the differential equation on the two sides of the juncture point.

A finite-difference representation is shown in Fig. 2 with a jump occurring immediately ahead of point 3 and point "a" located immediately ahead of the juncture point. In order to formulate difference representations of the derivatives at point 3, Taylor's series representations are employed which avoid any series expansions across the discontinuity.

Thus, a Taylor's series expansion is used from point 3 to 4 and from points "a" to 2. Points "a" and 3 across the discontinuity are then related through the jump conditions of Eqs. (10c) and (10d) to yield

$$\left(\frac{dR}{ds}\right)_3=\frac{R_4-R_2}{\Delta[1+K_1-(\Delta/2)K_2]}+\frac{\Delta K_3}{2[1+K_1-(\Delta/2)K_2]}+O(\Delta^2) \tag{11a}$$

$$\left(\frac{d^2R}{ds^2}\right)_3=\frac{(R_2-R_3)+(K_1-(\Delta/2)K_2)(R_4-R_3)}{(\Delta^2/2)[1+K_1-(\Delta/2)K_2]}-\frac{2K_3}{\Delta^2[1+K_1-(\Delta/2)K_2]}+O(\Delta) \tag{11b}$$

which reduce to the familiar central difference operators at nonjump points ($K_1=1$, $K_2=K_3=0$). Use of these operators to solve numerically the foregoing problem is straightforward with one example result presented in Fig. 3. Here the model shock slope, dR/ds, is shown for solutions obtained over $s=0$ to $s=2.5$ with the coefficients α_1 and α_2 taking the jump values shown at $s=0.9$ and $K_1=1.2$. It is seen that solutions obtained using the jump operators virtually reproduce the exact solution, while those obtained without the jump conditions suffer significant error over the entire range of integration.

Also, note that, while the second derivative operator of Eq. (11b) is formally first-order accurate, it is verified in Ref. 10 that this local truncation error does not destroy the global second-order accuracy of the solution obtained.

Application and Overall Method of Solution for FVSL

The numerical technique discussed earlier was applied to the solution of the full viscous shock-layer (FVSL) equations for hypersonic flow past spherically blunted cones. The overall method of solution for this case was as follows. Based on an initial assumed shock shape, the derivatives of the shock distance were evaluated using difference schemes that avoid any differencing across the juncture point. The first time sweep equations were then solved by starting at the stagnation point, where the governing equations reduce to ordinary differential equations. The first equation solved was the energy equation so that thereafter all quantities such as viscosity related to temperature could be evaluated. Next, the s-momentum equation was integrated to determine a u-velocity profile, and then the continuity equation was solved to determine first the shock standoff distance from Eq. (4) and then the v component of the velocity from Eq. (1a). Finally, Eq. (1d) was integrated to determine the local pressure level. The coefficients in the governing equations were then re-evaluated using the new flow variables. Repetition of the preceding steps at a given station continued until the solution converged. The method then stepped along the body surface and iterated at each station to achieve converged solutions.

Once the preceding method had passed over the downstream extent of the mesh, the second time step equation was invoked. The final sweep equation [Eq. (8b)] was then solved using the two boundary conditions of Eqs. (9). No iteration of the final sweep equation is required since it is linear. However, note that the final sweep equation requires the necessary jump conditions associated with the first derivative of the shock standoff distance, dR/ds, and also that associated with the second derivative, d^2R/ds^2. These jump conditions were evaluated using the flow properties obtained in the first sweep calculation. The shock shape obtained from the final sweep was then used to solve the next star sweep in time. The procedure continued in time until two alternate final sweeps converged to a desired degree of accuracy.

The numerical calculations reported in this paper utilized a convergence criteria of 0.01% accuracy in surface pressure and surface normal velocity gradient for local iterations and 0.1% accuracy in shock shape for global iterations. A typical calculation requires nearly 20-30 local iterations and approximately 15 time cycles to achieve these convergence criteria. The calculations in general required 10-15 min of computing time on an IBM 370.

Results and Discussion

The concepts developed in the preceding sections were used to obtain numerical solutions of the full viscous shock-layer equations for spherically blunted cones with cone half-angles varying from 30 deg to 0 deg at various Reynolds numbers. Initial interest was centered on verification of the concept through comparison at very high Reynolds numbers with inviscid surface pressures obtained with the method of characteristics. The first case considered was that of a 30 deg-half-angle spherically blunted cone at $M_\infty = 10$, $Re_\infty = 3 \times 10^5$, and $T_w/T_\infty = 0.05$, a case for which the inviscid calculations of Inouye et al.[11] were available. As discussed in Ref. 10, these high Reynolds number cases have very thin viscous layers and care was taken to insure that at least 10-15 grid points of the finite-difference mesh were in the boundary-layer region.

In order to assess the direct impact of the juncture region analysis on the shock-layer solutions, three levels of approximation were considered and compared with the inviscid

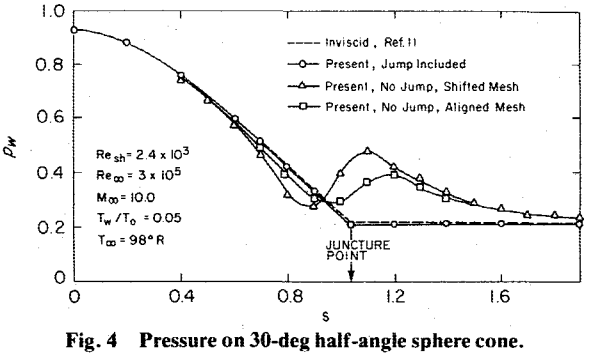

Fig. 4 Pressure on 30-deg half-angle sphere cone.

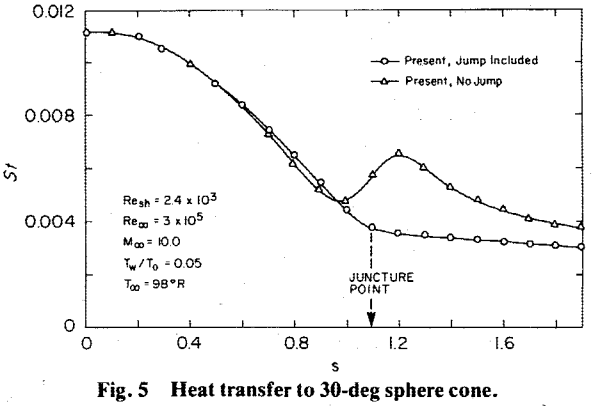

Fig. 5 Heat transfer to 30-deg sphere cone.

surface pressure distribution in Fig. 4. The first level (identified by triangles) completely ignored the relevant bow-shock juncture point jump conditions.§ These jump conditions are ignored by setting $K_1 = 1$ and $K_2 = K_3 = 0$ in Eqs. (11) while the flow variable derivative jumps are ignored by arranging the finite-difference grid so that the juncture point lies between two grid points (here $\Delta s = 0.1$). The resulting pressure distributions are seen in Fig. 4 to compare poorly with the inviscid calculations of Inouye et al.[11] especially near the downstream of the juncture point where the effects of curvature discontinuity are important. A 50% error in pressure is observed at the peak, and the error is seen to be felt from a half nose radius upstream of the corner to a full nose radius aft of the corner. The second level of approximation accounted for only the flow derivative jumps by adjusting the finite-difference grid so that the juncture point coincided with one of the grid points. This result is shown in Fig. 4 (designated by the squares) where the error is reduced from that of the first approximation but is nonetheless still unacceptable. Finally, the third approximation (identified by circles) incorporates the shock jump conditions in the finite-difference formulation as well as assures alignment of the grid system with the juncture point. This level of approximation is equivalent to eliminating all of the numerical errors associated with the juncture discontinuity and should implicitly contain the asymptotic analysis of Messiter and Hu.[12] The computed pressure distribution is seen to compare well with the inviscid calculations of Inouye et al.,[11] indicating that the adverse numerical effects associated with such a juncture discontinuity have been properly overcome. Moreover, it is seen that the present results virtually reproduce the inviscid pressure gradient discontinuity for this high local Reynolds number case. It is shown in Ref. 10 that, for this configuration, the scale length of the interaction effects predicted by the analysis of Messiter and Hu[12] would be so small as to produce a virtual discontinuity to the scale displayed in Fig. 4.

§Note that throughout this discussion the phrase "jump conditions" does not refer to the Rankine Hugoniot conditions but rather to the shock shape derivative jumps typified by Eq. (6).

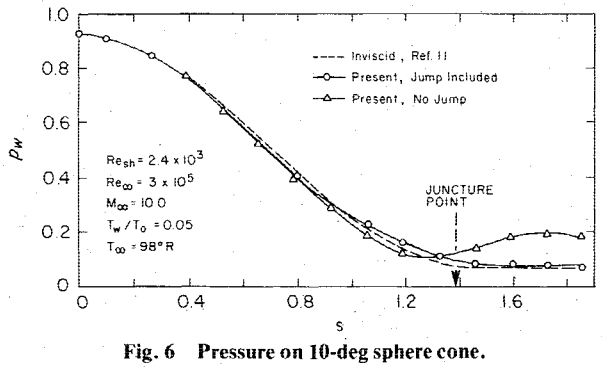

Fig. 6 Pressure on 10-deg sphere cone.

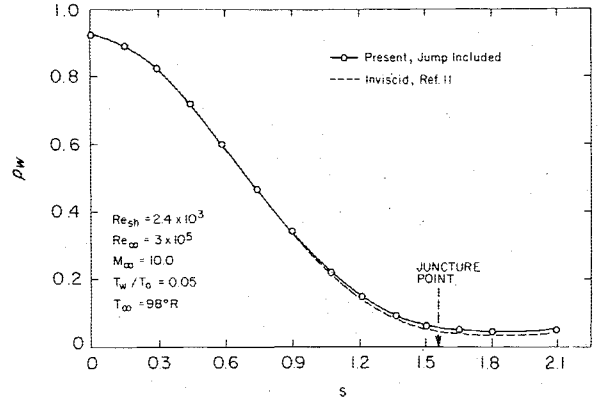

Fig. 7 Pressure on sphere cylinder.

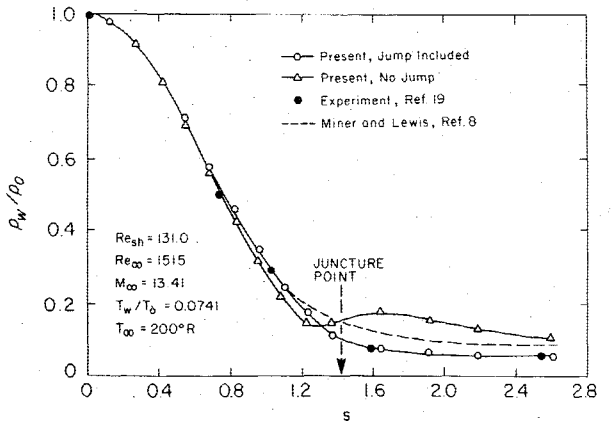

Fig. 8 Pressure on 7.5-deg sphere cone.

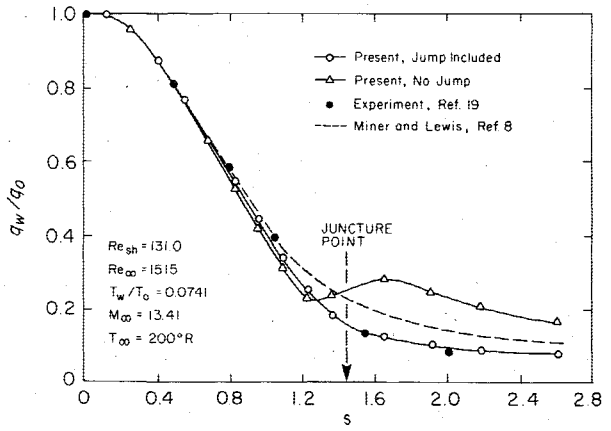

Fig. 9 Heat transfer to 7.5-deg sphere cone.

The surface heat-transfer distributions for the first and third approximations studied in the foregoing are shown in Fig. 5, these representing the least and most accurate approaches, respectively. Again, it is seen that large differences occur in the solution when the adverse affect associated with the curvature discontinuity is ignored. Based on the comparison presented in Fig. 4 it is assumed here that the heating level calculated with the jump effect included is the more accurate of the two—thus indicating enormous errors in the calculation made ignoring the jumps.

To test the generality of the preceding conclusion, solutions were obtained for lower cone half-angles. Such results were obtained by reducing the cone angle in increments of approximately 5 deg with the number of mesh points between the juncture and stagnation point kept fixed, resulting in a slight increase in the longitudinal step size Δs as the cone angle was reduced. Figures 6 and 7 present the resulting surface pressure distributions for cone angles of 10 deg and 0 deg for the first (least accurate) and third (most accurate) approximations identified earlier. It is noted that, in all cases, the predicted surface pressure distribution compares favorably with the inviscid calculations of Inouye et al.[11] when the proper jump effects associated with longitudinal derivatives (for both the flow and shock) are accounted for in the solution scheme. It is also clear from the figures that, when such jump effects are ignored in the calculation unacceptable error levels are encountered. Note that Fig. 7 for a 0-deg cone angle (a sphere cylinder) does not contain results corresponding to the no-jump approximation case. This is because the errors were so large at the juncture point that a properly converged numerical solution could not be obtained for this case—again underscoring the seriousness of the errors encountered in not properly accounting for the jump conditions. To date most viscous shock-layer methods have encountered severe numerical difficulties for sphere-cone half-angles lower than 20 deg due to large shock-layer thickness associated with such bodies. The present technique is seen to predict flow properties for cone-angles as low as 0 deg for which case the shock-layer thickness is found to be large.

Thus far it has been shown that the present approach yields good comparisons with the inviscid theory[11] at high Reynolds numbers. Comparisons are now presented with experimental data for spherically blunted cones at a moderate Reynolds number where viscous interaction effects become more important. The case considered is that of flow over a 7.5-deg half-angle spherically blunted cone at $M = 13.41$, $Re_\infty = 1515$, $T_w/T_0 = 0.0741$, and $T_\infty = 200°R$ corresponding to the experimental data of Pappas and Lee.[19] Numerical solutions for this case were obtained by first choosing a normal step size $\Delta\eta$, which insured enough points within the viscous layer and by choosing Δs, such that a mesh point of the finite-difference scheme was coincident with the juncture point (see Ref. 10 for details). These results are presented in Figs. 8 and 9 along with the experimental results and independent numerical calculations by Miner and Lewis.[8] The first case shown (indicated by triangles) did not include the effect of the shock jump conditions whereas the second case (indicated by circles) did. Figures 8 and 9 show that the latter of these two gave excellent agreement with the experimental data while the first produced serious errors. Also shown are the results presented by Miner and Lewis[8] for the same body but with the surface curvature artificially smoothed in the juncture region. While there is a reduction in error as observed in Figs. 8 and 9, this approach is seen still to misrepresent the experimental results, especially aft of the juncture point.

The final test case considered was that of a 4-deg half-angle spherically blunted cone at $M_\infty = 9.82$, $Re_\infty = 9905$, $T_w/T_0 = 0.5$, and $T_\infty = 98.3°R$ corresponding to the experimental conditions reported in Ref. 20. Both pressure and heat-transfer data were reported aft of 7 nose radii on this body and theoretical calculations were presented based on the

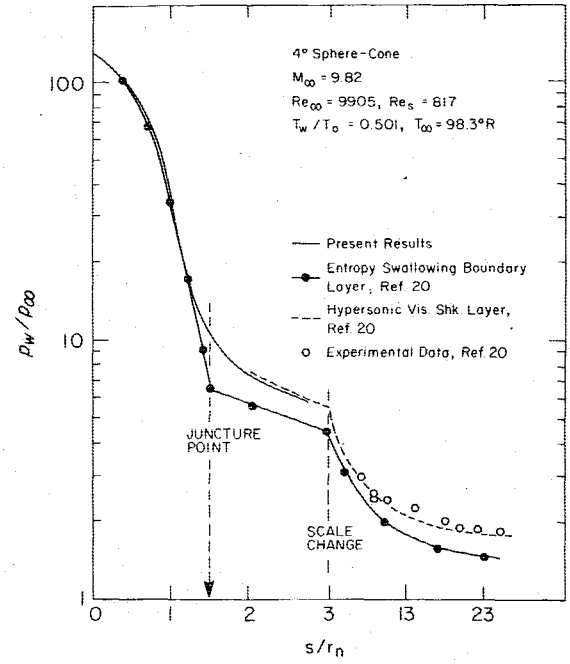

Fig. 10 Pressure on 4-deg sphere cone.

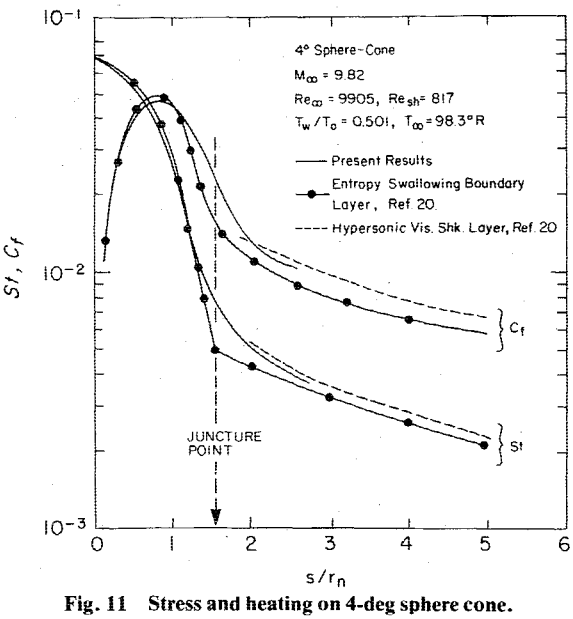

Fig. 11 Stress and heating on 4-deg sphere cone.

viscous shock-layer technique of Lubard and Helliwell.[21] However, these later solutions were restricted to the cone portion of the body and an approximate technique based on an entropy swallowing approach was used to obtain the nose region solutions (see Ref. 20 for details).

The surface pressure distributions for this case are presented in Fig. 10. The hypersonic viscous shock-layer solutions (HVSL) of Ref. 20 were obtained using an inviscid surface pressure distribution to obtain entropy swallowing higher-order boundary-layer solutions up to the juncture point where an abrupt switch was made to the Lubard and Helliwell[21] code for conical geometry. The resulting solutions are seen to compare well with the experimental data far downstream on the cone portion of the body. However, this calculation was not considered reliable in the immediate juncture region[20] since initial data were obtained from entropy swallowing boundary-layer calculations. In order to resolve this issue, the present method was applied over the nose region of the body and is shown in Fig. 10 to provide a smooth transition across the juncture region onto the cone portion of shock-layer solutions. This indicates that the error associated with the juncture point due to an abrupt change from the entropy swallowing boundary layer to a shock-layer approach using the Lubard and Helliwell code[21] is restricted to within about 1-2 nose radii downstream of the juncture point. This trend is also observed in earlier present calculations (such as in Fig. 4) where error associated with the juncture point tend to diminish within about 2-3 nose radii downstream of the juncture point.

Figure 11 shows the skin friction coefficient and the Stanton number distribution for the case considered in the foregoing. Here again, the present results are seen to provide a smooth transition over the juncture region to the shock-layer solutions obtained using the Lubard and Helliwell code.[21] The entropy swallowing boundary-layer calculations[20] are seen to misrepresent the juncture region severely.

Conclusions

An analysis of the physical flow behavior at the sphere/cone tangency point indicates that, independent of the choice of the coordinate system, inviscid theory would predict a discontinuity in the flow gradients only on the surface of the body at the sphere/cone juncture point. However, from the analysis of Messiter and Hu,[12] it was found that in the limiting case of very high Reynolds number this discontinuity would be smoothed out by the sublayer interaction effect within the inner scale length. In addition, it was found that the use of a surface coordinate system introduces discontinuities in the flow gradients relative to surface distances everywhere across the shock layer at the juncture point. Analytical jump conditions have been developed at the sphere/cone juncture point for the discontinuous flow gradients associated with the choice of a surface coordinate system. Finite-difference expressions were then developed that accounted for these embedded gradient discontinuities in order to eliminate numerical difficulties in the solution of the full viscous shock-layer equations. Such solutions were obtained by a numerical scheme which utilized a time-dependent relaxation technique for the bow shock wave shape. Comparisons of the present results with inviscid solutions at high Reynolds numbers and experimental data at intermediate ones were found to be good. Results were presented that indicated that without proper accounting of the curvature effects, large errors in the surface properties will be produced over a significant ($\pm$ 1 nose radii) portion of a sphere/cone surface.

Acknowledgment

This research was supported through the Arnold Engineering Development Center, under Contract No. F40600-74-C-0011 with Elton Thompson as Air Force Project Engineer. The authors wish to express their thanks to J. C. Adams and A. W. Mayne of ARO, Inc. for helpful technical discussions during the course of this study.

References

[1] Jain, A. C. and Adimurthy, V., "Hypersonic Merged Stagnation Shock Layers, Part I, Adiabatic Wall Case," *AIAA Journal*, Vol. 12, March 1974, p. 355.

[2] Jain, A. C. and Adimurthy, V., "Hypersonic Merged Stagnation Shock Layers, Part II, Cold Wall Case," *AIAA Journal*, Vol. 12, No. 3, March 1974, pp. 348-354.

[3] Van Dyke, M., "A Review and Extension of Higher Order Hypersonic Boundary-Layer Theory," *3rd International Symposium on Rarefied Gas Dynamics*, Paris, France, June 1962.

[4] Davis, R. T., "Numerical Solution of the Hypersonic Viscous Shock Layer Equations," *AIAA Journal*, Vol. 8, May 1970, pp. 843-851.

[5] Srivastava, B. N., Werle, M. J., and Davis, R. T., "Solution of the Hypersonic Viscous Shock Layer Equations for Flow Past a Paraboloid," *AIAA Journal*, Vol. 14, Feb. 1976; also Dept. of

Aerospace Engineering, Univ. of Cincinnati, Rept. No. AFL-74-4-10, April 1974.

[6]Srivastava, B. N., Werle, M. J., and Davis, R. T., "Stagnation Region Solutions of the Full Viscous Shock Layer Equations," *AIAA Journal*, Vol. 14, Feb. 1976; also Arnold Engineering Development Center, Tenn., Rept. No. AEDC-TR-76-53, Aug. 1976; also *11th Southeastern Seminar on Thermal Sciences*, Univ. of Tennessee, April 28-29, 1975.

[7]Davis, R. T. and Nei, Y. W., "Numerical Solution of the Viscous Shock Layer Equations for Flow Past Spheres and Paraboloids," Sandia Corp., Final Rept., Contract No. 48-9195, 1970.

[8]Miner, E. W. and Lewis, C. H., "Hypersonic Ionizing Air Viscous Shock Layer Flows Over Sphere Cones," *AIAA Journal*, Vol. 13, Jan. 1975, pp. 80-88.

[9]Werle, M. J., Srivastava, B. N., and Davis, R. T., "Numerical Solutions to the Full Viscous Shock Layer Equations Using an ADI Technique," Dept. of Aerospace Engineering, Univ. of Cincinnati, Rept. No. AFL 74-7-13, Aug. 1974.

[10]Srivastava, B. N., Werle, M. J., and Davis, R. T., "Viscous Shock Layer Solutions for Hypersonic Sphere-Cones," Arnold Engineering Development Center, Tenn., AEDC-TR-77-20, Jan. 1977; also Ph.D. Dissertation (B. N. Srivastava), Univ. of Cincinnati, Aerospace Engineering, Dept., 1976.

[11]Inouye, M., Rakich, J., and Lomax, H., "A Description of Numerical Methods and Computer Programs for Two Dimensional and Axi-symmetric Supersonic Flow Over Blunt Nosed and Flared Bodies," NASA TND-2970, Aug. 1965.

[12]Messiter, A. F. and Hu, J. J., "Laminar Boundary Layer at a Discontinuity in Wall Curvature," *Quarterly Journal of Applied Mathematics*, July 1975, pp. 175-181.

[13]Delliger, T. C., "Nonequilibrium Air Ionization in Hypersonic Full Viscous Shock Layers," AIAA Paper 70-806, June 1970.

[14]Cheng, H. K., "The Blunt-Body Problem in Hypersonic Flow at Low Reynolds Number," Cornell Aeronautical Laboratory, Rept. AF-1285-A-10, 1963.

[15]Davis, R. T. and Flügge-Lotz, I., "Second-Order Boundary Layer Effects in Hypersonic Flow Past Axisymmetric Blunt Bodies," *Journal of Fluid Mechanics*, Vol. 20, Part 4, 1964, pp. 593-623.

[16]Anderson, E. C., Moss, J. N., and Sutton, K., "Turbulent Viscous Shock-Layer Solutions with Strong Vorticity Interaction," AIAA Paper 76-120, Wash., D.C., Jan. 1976.

[17]Moss, J. N., "Reacting Viscous Shock-Layer Solutions with Multicomponent Diffusion and Mass Injection," AIAA Paper 74-73, Wash., D.C., Jan. 1974.

[18]Carnahan, B., Luther, H. A., and Wilkes, J. O., *Applied Numerical Methods*, John Wiley & Sons, New York, 1969.

[19]Pappas, C. C. and Lee, G., "Heat Transfer and Pressure on a Hypersonic Blunt Cone with Mass Addition," *AIAA Journal*, Vol. 8, May 1970, pp. 954-956.

[20]Mayne, A. W., Jr., Private communique, Aug. 1976; also "Calculation of the Laminar Viscous Shock Layer on a Blunt Biconic Body at Incidence to Supersonic and Hypersonic Flow," AIAA Paper 77-88, Los Angeles, Calif., Jan. 1977.

[21]Lubard, S. C. and Helliwell, W. S., "Calculation of the Flow on a Cone at High Angle of Attack," *AIAA Journal*, Vol. 12, July 1974, pp. 965-974.